Available online at www.sciencedirect.com

SciVerse ScienceDirect

Journal of the European Ceramic Society 32 (2012) 649–655

www.elsevier.com/locate/jeurceramsoc

Processing of thin film ceramic membranes for oxygen separation

Jonas Gurauskis *, Ørjan Fossmark Lohne, Hilde Lea Lein, Kjell Wiik

Department of Materials Science and Engineering, Norwegian University of Science and Engineering, Sem Sælandsvei 12, NO-7491 Trondheim, Norway

Received 18 July 2011; received in revised form 28 September 2011; accepted 1 October 2011
Available online 21 October 2011

Abstract

Processing of dense and thin ceramic membrane layers for high temperature selective oxygen separation is addressed in this study. Mixed oxygen-ionic and electronic conducting perovskite oxide system based on $La_{0.2}Sr_{0.8}Fe_{0.8}Ta_{0.2}O_{3-\delta}$ composition is employed for processing of structural and functional layers. Special focus is aimed at obtaining thin layer and final microstructure with particle size in the sub-micron range. Thin layer deposition is performed by dip coating technique using stable colloidal suspension of perovskite particles dispersed within ethanol media. Two polymer based surfactants were screened for their effect on particle agglomeration and rheological response. By using optimum quantity of 2.5 wt.% addition of selected surfactant it is possible to obtain dense 15–60 μm thick functional layers. The thermal cycle applied resulted in final particle sizes within sub-micron range. By employing suspension with pore former it was possible to significantly increase the surface area of the functional layer.

Keywords: A. Suspensions; A. Films; A. Shaping; D. Perovskites; E. Membranes

1. Introduction

Dense ceramic membranes made from mixed oxygen-ionic and electronic conducting (MIEC) perovskite oxides are attracting a lot of interest due to their promising potential as a reliable source for oxygen and syngas production.[1–3] These membranes operate at high temperatures (700–900 °C) permeating 100% pure oxygen directly from air eliminating the need for expensive conventional cryogenic technology. And in principle this membrane technology can even be integrated directly in catalytic process reactors thus performing the oxygen separation and catalytic process in a single step.

Extensive reviews by Sunarso et al. [4] and Hashim et al. [5] compile the theoretical principles behind this technology and summarize the latest achievements in this area, reflecting extensive interest both from industry and academia.

Given the material composition there are two simple approaches to optimize the oxygen permeation flux across a dense MIEC material. Firstly, reduce the bulk diffusion contribution by decreasing the thickness of the membrane below the critical value and, secondly, increase the surface area available for surface exchange reactions to take place. This leads to an asymmetric-structured membrane architecture composed of a porous structural support and a thin dense functional layer with preferably large surface area.[3,6,7] But, as noted by Hendriksen et al. [3] and Lein et al.[8] the reducing conditions present at membrane operating conditions may be followed by dimensional instability of perovskite materials. This can lead to the delamination between structural porous support layer and thin dense functional layer. As a consequence many research groups take a great effort to find the best dopants for perovskite based compounds to achieve both elevated oxygen permeation flux and structural stability under harsh membrane operating conditions.[4,5]

In order to evaluate and employ possible MIEC candidate materials the reliable conformation route should be established to obtain membrane structures with desired geometry and controlled microstructure. Even so, very few reports can be found on preparation of defect free thin film (thickness lower than 25 μm) membranes.[7,9]

In this study the colloidal processing route based on dip coating was approached to perform the deposition of thin $La_{0.2}Sr_{0.8}Fe_{0.8}Ta_{0.2}O_{3-\delta}$ (LSFTa) composition functional layers. Dip coating technique was chosen due to its simplicity and the possibility to carry out geometrically independent layer deposition on porous supports without unnecessary

* Corresponding author. Tel.: +47 735 94079; fax: +47 735 50203.
E-mail address: jonas.gurauskis@material.ntnu.no (J. Gurauskis).

0955-2219/$ – see front matter © 2011 Elsevier Ltd. All rights reserved.
doi:10.1016/j.jeurceramsoc.2011.10.009

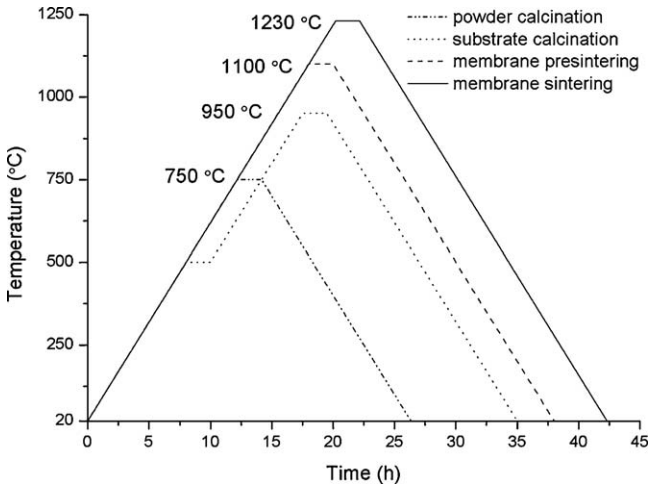

Fig. 1. Thermal treatment cycles applied to LSFTa material during membrane processing steps. All cycles were performed in stagnant air atmosphere.

complications of the process in both lab and on an industrial scale.[10] Polymeric based commercial surfactants were selected for perovskite phase stabilization within solvent due to their low residual ash content as stated by the suppliers. Although presenting more challenges with respect to colloidal stabilization,[11,12] the starting LSFTa powder with primary particle size within nanometric range was chosen. This will result in a smaller grain size within the final thin layer microstructure thus less prone to critical defect formation.[13] As suggested by Ikeguchi et al. [14] deposition of thin film functional layers was done on porous substrates of the same composition in order to avoid defect formation due to thermal expansion coefficient mismatch and unwanted solid state reactions.

2. Materials and methods

The $La_{0.2}Sr_{0.8}Fe_{0.8}Ta_{0.2}O_{3-\delta}$ (LSFTa) composition powder employed in this work was prepared by spray pyrolysis and delivered by CerPoTech A.S.[15] The as received powder (powder precursor) was calcined (Fig. 1) at 750 °C to eliminate residual organic components as well as secondary phases. The calcined powder was used as the feed stock for all experiments in the present study. Phase purity of powders and sintered samples were routinely checked by means of X-ray diffraction using Bruker D8 diffractometer. Particle size distribution was evaluated by laser diffraction technique in aqueous media using Mastersizer 2000 (Malvern Instruments, UK). Specific surface area of powder was measured using BET method with Tristar 3000 analyser from Micromeritics. Reagent grade ethanol (Sigma–Aldrich) was used as the solvent carrier. Hypermer KD-1 (surfactant 1) was provided by Croda Inc.Plc. and Dolacol D1003 (surfactant 2) was provided by Zschimmer & Schwarz GmbH.

Suspensions were ball-milled in polystyrene bottles with zirconia ball-milling media. Milling was done during 24 h and prepared suspensions were left slow rolling for further 24 h for further stabilization. Zeta potential of prepared suspensions was measured using electrokinetic light scattering technique with Zetasizer NS (Malvern Instruments). Standard disposable cells were filled with supernatants of optimum concentrations for measurement and 15 runs were performed for each composition. Rheological characterization of suspensions with solid load of 2 vol.% in all cases was done with rotational rheometer Mars III (Haake, Karlsruhe) equipped with double cone-and-plate test geometry (titanium double cone of 1°, ∅ = 60 mm). Viscosity values were recorded using controlled shear stress mode (CS) at low-shear range and switching to controlled share rate (CR) mode within the shear range above 30 s^{-1}. Flow curves of samples were recorded on separate runs using controlled share rate (CR) mode up to 500 s^{-1} and dwell time of 30 s at maximum shear. All measurements were carried out at a temperature of 20 ± 0.1 °C and precautions were taken to perform measurements on suspensions at rest with fully recovered structure.

Optimized suspensions were deposited by dip coating on 25 mm diameter membrane supports, which were made by double action uniaxial pressing of LSFTa powder containing 20 wt.% carbon black (Merck KGaA) as a pore former. Prior to deposition, supports were calcined at 950 °C (Fig. 1) to eliminate pore former and to gain some structural strength. Supports were attached to glass strips to limit the deposition of dense layer just to one side. Suspensions with varying solid load were screened within the range from 0.5 to 2.0 vol.% in order to adjust the thickness of dip coated layer. Pre-sintering and sintering thermal treatment cycles of samples are summarized in Fig. 1. Corn starch (Remy DR-LA, Ferrer Alimentacion S.A.) with particle size distribution between 2 and 8 μm was used as pore former for suspensions dedicated to surface area modification. 30 wt.% pore former was added to the optimized suspension with 0.5 wt.% solid load and its deposition was done by a single dip coating cycle.

Starting powders and obtained microstructures were investigated with a Hitachi S3500 N scanning electron microscopy (SEM). The existence of defects within dense LSFTa layer leading to gas leaks was assessed by He overpressure method at room temperature. During this test the thin film membrane sample is placed between two gas chambers using rubber rings for sealing. He gas at 100 ml/min flow rate and ~1.3 atm pressure is supplied to one chamber while argon gas is supplied to the opposite chamber at 100 ml/min flow rate and ~1.1 atm pressure. Exhaust of argon gas was analyzed for He presence using Varian Micro-GC CP4900 gas chromatographer with argon as a carrier gas.

3. Results

Fig. 2 shows XRD of feed stock powder (calcined powder precursor) as well as samples sintered at 1100 and 1230 °C. Formation of single phase LSFTa perovskite structure is evident from diffractograms after exposing the samples to temperatures of 1100 °C and above. Specific surface area of calcined powder was measured to be ~13.2 m^2/g, and assuming spherical shape of the particles combined with the theoretical density of LSFTa, $\rho_{LSFTa} = 6.3\ g/cm^3$, the average size of primary particles was calculated to be ~84 nm.

Fig. 3 shows the Zeta potential (ζ) corresponding to LSFTa particles suspended in ethanol and the effect caused by the use

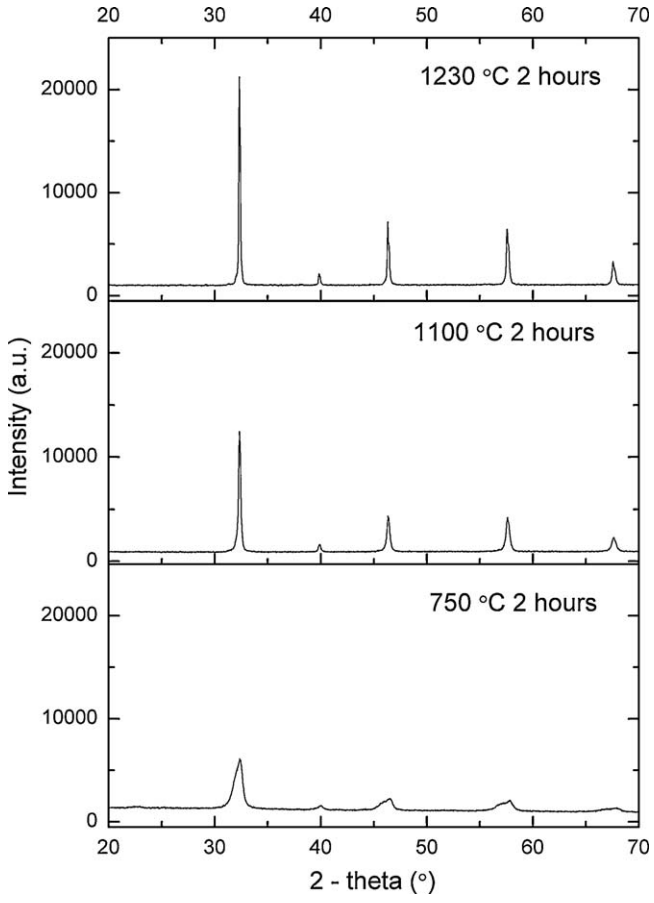

Fig. 2. X-ray diffraction data corresponding to LSFTa phase after thermal treatment cycles applied to LSFTa material during membrane processing steps.

of two different surfactants. In absence of surfactants the ζ-potential is seen to be positive with an average value of 25 mV however exhibiting a large standard deviation. Addition of surfactant 1 resulted in a gradual decrease in standard deviation values with increasing surfactant content, but caused little effect on the overall ζ-potential value. It remains positive within the whole range of surfactant concentration showing ~30 mV at 3.0 wt.% surfactant added. As for the surfactant 2, a change from the positive to negative sign was observed, reaching the maximum absolute values of ~25 mV in the case of addition above 2.0 wt.%. It is evident from Fig. 3 that the presence of surfactant 2 also reduces the standard deviation of the ζ-potential significantly.

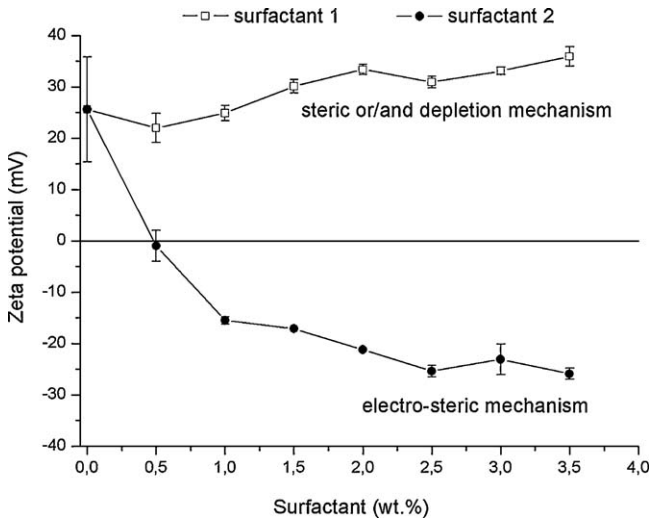

Fig. 3. Zeta potential values corresponding to LSFTa particles suspended in ethanol as a function of surfactant content.

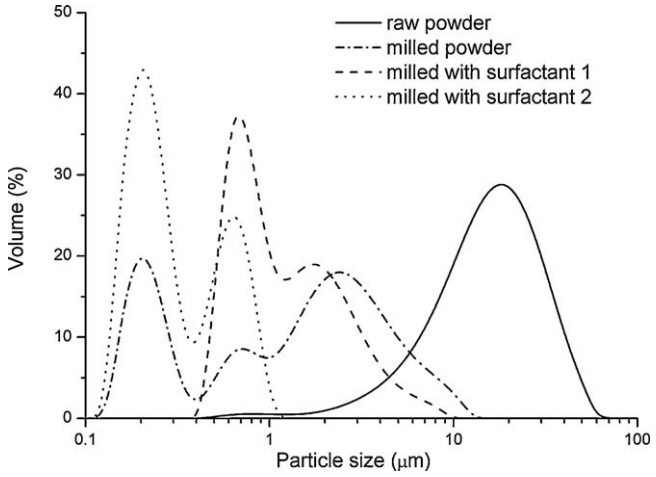

Fig. 4. Effect of surfactants with corresponding optimum quantity on particle size distribution after ball milling step. The lowest degree of agglomeration was observed for surfactant 2, leading to primary agglomerates at ca. 200 nm.

Based on the ζ-potential data, further work was performed with the 2 vol.% solid load suspensions stabilized with surfactant quantities corresponding to the highest ζ-potential. Particle size distribution corresponding to these suspensions after ball milling step during 24 h is shown in Fig. 4. For comparison reasons particle size distribution of LSFTa powder without surfactants, as well as with surfactants added prior to milling are plotted as well. LSFTa powder in the absence of surfactants shows strong agglomeration corresponding to agglomerates of ~20 μm. Milling of this powder in the absence of surfactants comminute the largest agglomerates but re-agglomeration also takes place. Fig. 4 shows that surfactant 1 shifted the main peak from 2 μm to approx. 0.7 μm. Surfactant 2 was able to reduce the re-agglomeration even more and resulted in a particle size distribution with the largest volume fraction at approx. 0.2 μm.

Fig. 5 shows SEM micrographs corresponding to LSFTa powder before and after milling. Prior to milling the presence of shell type agglomerates of ~20 μm size are evident (Fig. 5a). Milling without adding surfactants results in re-agglomeration of primary particles (Fig. 5b). Most significant reduction in observed re-agglomeration is achieved by the presence of surfactant 2 (Figs. 4 and 5c).

Based on particle size distribution data (Fig. 4) and direct observation of LSFTa powder agglomeration by SEM (Fig. 5c), further work was concentrated on colloidal suspension systems with surfactant 2. The screening for optimum surfactant 2 content was done in suspensions with the 2 vol.% solid load and surfactant quantity within the range of 2–3 wt.% of solid load. Fig. 6 represents viscosity value curves as a function of applied shear. All suspensions show shear-thinning behavior and viscosity values above 10 mPas at zero-shear viscosity plateau range.

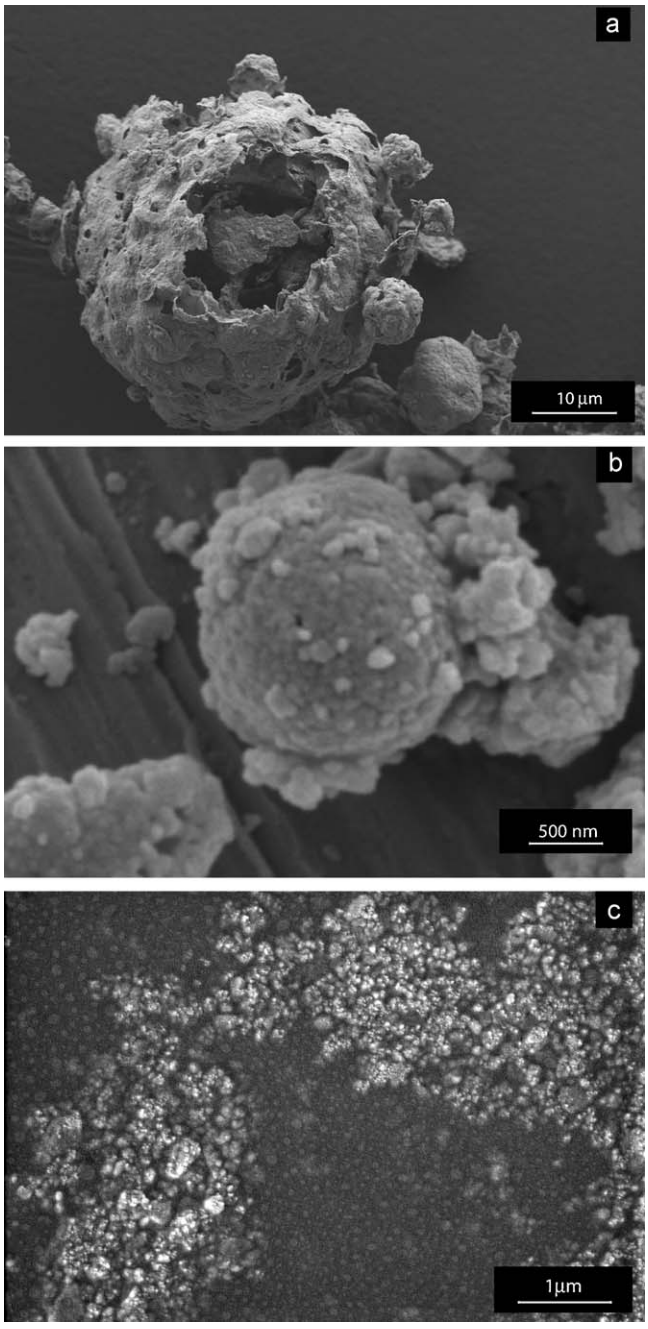

Fig. 5. SEM micrographs of LSFTa powders; (a) powder as received from spray pyrolysis, (b) powder milled for 24 h and (c) powder milled for 24 h with surfactant 2.

Varying surfactant 2 quantities between 2 and 3 wt.% showed a local viscosity minima at 2.5 wt.% in all applied shear range. As seen from the inclusion in Fig. 6, the viscosity shows the trend to decrease with increasing surfactant content up to 2.5 wt.% and rise with further surfactant content increase.

Flow curves (Fig. 7) showed the formation of hysteresis between upward and downward segments for all concentrations of surfactant 2, consistent with thixotropic behavior. The lowest thixotropic area calculated was for surfactant concentration 2.5 wt.%.

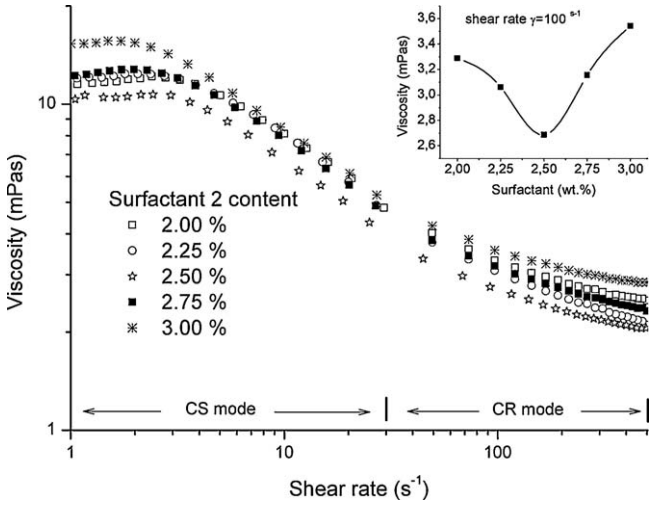

Fig. 6. Shear viscosity values as a function of shear rate corresponding to suspensions with varying content of surfactant 2 (inclusion shows the viscosity values at a fixed shear rate of 100 s^{-1}). The lowest shear viscosity values are obtained for 2.5 wt.% surfactant concentration.

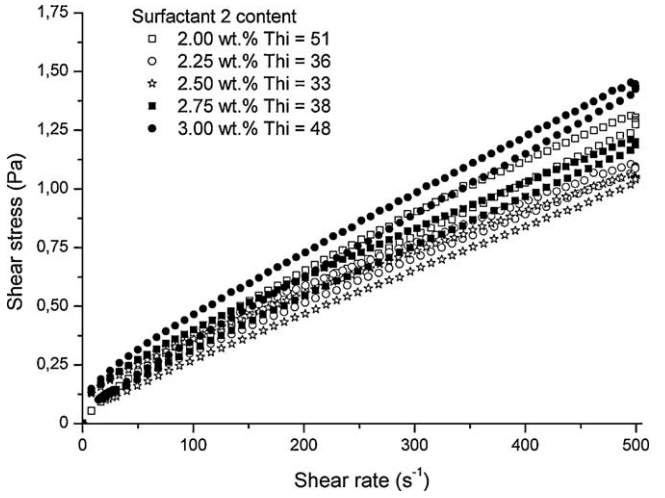

Fig. 7. CR mode flow curves and corresponding thixotropy values measured for suspensions with varying content of surfactant 2. Lowest hysteresis area is observed for suspension with 2.5 wt.% surfactant concentration.

Following the results obtained from the rheology study (Figs. 6 and 7), deposition by dip coating of thin functional layers with LSFTa composition powder was performed using suspensions with surfactant 2 concentration of 2.5 wt.% of solid load. Sintered functional layer thickness corresponding to single 10 s deposition of the suspensions with varying solid loads are summarized in Table 1. Suspension with the highest solid

Table 1
Thickness values of obtained LSFTa layer after single dip coating step as a function of suspension solid load.

Solid loading (vol.%)	Thickness (µm)	Layer appearance
0.50	15 ± 1	
0.75	27 ± 3	Defect free coatings
1.00	51 ± 3	
2.00	76 ± 5	Border peeling off

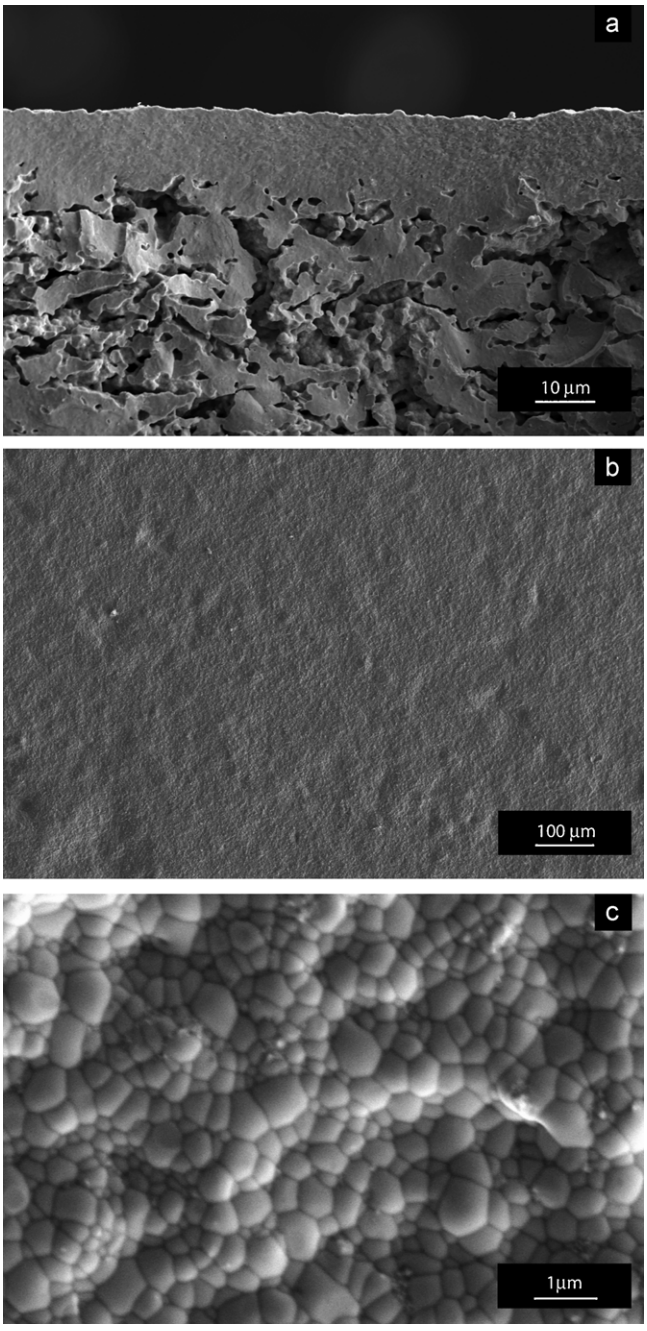

Fig. 8. FE-SEM micrographs of functional LSFTa layer obtained with 0.5 vol.% suspension after final sintering step; (a) fracture cross section shows dense ~15 μm thick layer, (b) top view of defect free layer and (c) detail of top view showing grain sizes below 1 μm.

load (2.0 vol.%) reached a thickness close to ~80 μm, while the lowest solid load suspension (0.5 vol.%) resulted in a film thickness of ~15 μm. In the case of the highest solid load (2.0 vol.%) defect formation in the form of "peeling of" close to planar support borders was observed.

For suspensions with lower solid load, dense and completely defect free layer was obtained. Fig. 8 shows SEM micrographs corresponding to dense LSFTa layer obtained with 0.5 vol.% solid load suspension. Fracture cross section (Fig. 8a) and top view (Fig. 8b) shows defect free ~15 μm thick layer. As

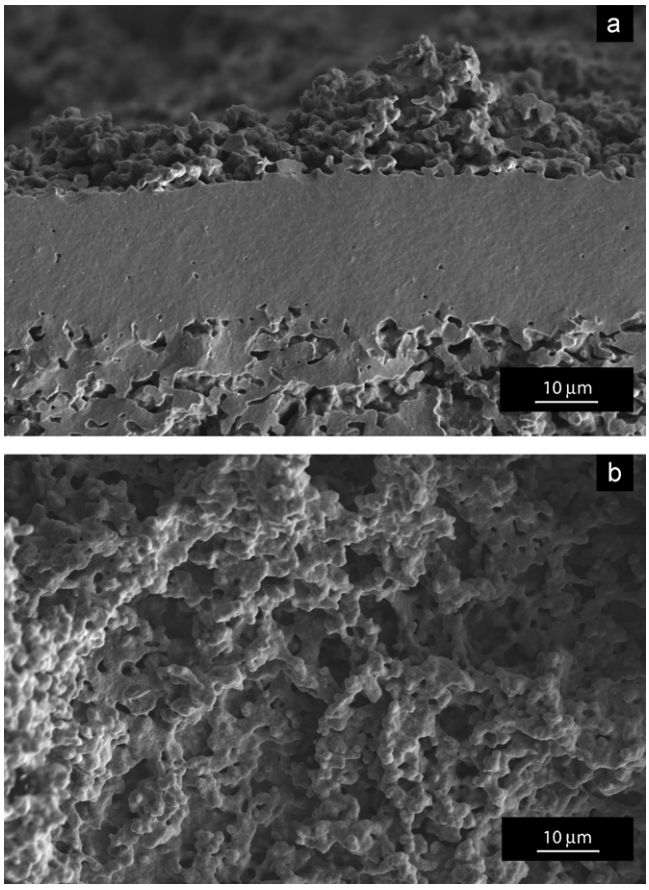

Fig. 9. FE-SEM micrographs of final functional LSFTa layer with surface modification; (a) fracture cross section shows dense ~20 μm thick layer with surface modification, (b) top view of surface modified side.

observed from Fig. 8c, the thin layer is composed of uniformly distributed fine grains (<1 μm).

Surface modification was done on presintered thin functional layer obtained with 0.5 vol.% solid load suspension. Deposition of starch modified suspension on presintered layers caused the formation of a top surface layer with high porosity after final sintering step. Fig. 9 shows SEM micrographs corresponding to microstructure of dense LSFTa layer with surface modification using starch modified suspension. Final dense layer thickness of ~20 μm (Fig. 9a) is obtained with highly porous surface modification layer on top (Fig. 9b).

He leakage check performed at room temperature on thin film (17–20 μm) dense membrane samples with smooth and rough surface structuring showed no trace of He leakage.

4. Discussion

The $La_{0.2}Sr_{0.8}Fe_{0.8}Ta_{0.2}O_{3-\delta}$ composition powder introduced to ethanol without use of any surfactant shows a positive ζ-potential charge (Fig. 3). This is attributed to adsorption of ethanol onto LSFTa surface, where the acidic nature of ethanol results in proton transfer to particle surface. During this process of dynamic adsorption and desorption the observed positive surface charge is generated.[16]

Adsorption of surfactant 1 on the surface of LSFTa particles showed gradual decrease in the standard deviation, however virtually no effect on the level of the Zeta potential. Completely opposite effect was observed in the case of surfactant 2 where, apart from a decrease in standard deviation, a shift in the ζ-potential from (+) to (−) was observed. The observed ζ-potential data indicate that in the case of surfactant 1, the stabilization mechanism generated will be mainly based on the formation of the steric barrier and/or a depletion mechanism. While in the case of surfactant 2, the formation of an electro-steric barrier is more likely.

A representative particle morphology of the LSFTa powder is given in Fig. 5a and shows the characteristic egg-shell agglomerates typical for spray pyrolized powder.[17] Both particle size distribution (Fig. 4) and direct SEM observation (Fig. 5b) confirm strong re-agglomeration of LSFTa primary particles (∼84 nm) in ethanol media during ball milling. Observed re-agglomeration indicates that observed positive charge on LSFTa particles and corresponding electrostatic repulsive forces are not efficient to reach suspension stability, thus signifying the need for surfactants to obtain stability within the colloidal system.[11,18] Incorporation of surfactant 1 during ball milling step showed little effect on system stability causing formation of primary particle agglomerates above 1 μm (Fig. 4). Incorporation of surfactant 2 resulted in bimodal distribution of particles as well, but agglomerate size was reduced significantly below 1 μm and average particle size of $d_{V50} = 0.2$ μm was reached. Large scale agglomeration observed in case of surfactant 1 indicates that the formed steric barrier layer may be insufficient to provide effective steric stabilization in the ethanol based system. In case of surfactant 2, where electro-steric stabilization mechanism is expected, higher stability of the colloidal system is reached compared with surfactant 1. Direct observation of ball milled LSFTa powder with surfactant 2 (Fig. 5c) does not show the presence of agglomerates within the size range of 0.7 μm which would correspond to the second peak as observed by laser diffraction (Fig. 4). The presence of these soft agglomerates can be attributed to possible flocculation by the bridging mechanism due insufficient effectiveness or/and inadequate amount of surfactant.[19] By combining these results surfactant 2 was selected for further study where optimization of surfactant content was performed by rheological characterization.

As observed in Fig. 6, concentration sweep of surfactant 2 between 2 and 3 wt.% of solid loading gave a minimum viscosity at 2.5 wt.% within the whole range of shear rates. Independent of surfactant concentration all suspensions show shear thinning behavior and typical low viscosity plateau at low shear stress indicating fine particle (below 1 μm) colloidal system. Taking into account that solid load concentration within the colloidal systems is very low (just 2 vol.%), the observed viscosity behavior can be explained by the presence of a significant degree of interaction/flocculation between the particles. Flow curves of these suspensions (Fig. 7) further confirm the presence of flocculation at rest due to positive hysteresis. As observed for the viscosity, the lowest thixotropic behavior is also observed at 2.5 wt.% of surfactant 2. Higher thixotropic values at lower surfactant content should be attributed to insufficient particle surface coverage by surfactant. Whereas, observed increase in thixotropy at higher concentrations is attributed to excess surfactant which results in interaction (cross linking) between already absorbed surfactant polymer chains.[19]

Following rheological characterization results, LSFTa powder suspensions for thin functional layer deposition by dip coating were prepared using 2.5 wt.% of surfactant 2. As reported in Table 1, it was possible to adjust the thickness of the functional layer by controlling the solid load of suspensions. For ∼80 μm thick layers, obtained with highest solid load, structural defect formation was detected. These thick layers curled close to sample edges by separating itself from the porous support. This can be attributed to a combination of different sintering rates and insufficient contact strength between dense layer and porous support at some stage in the sintering process. All other concentrations resulted in defect free and dense microstructures (Fig. 8b) reaching lowest thickness of ∼15 μm for 0.5 vol.% concentration suspension (Fig. 8a).

As expected, the use of LSFTa powder with small primary particles and optimized colloidal suspension resulted in fine grain microstructure materials with grain size distribution below 1 μm (Fig. 8c).

He overpressure method used to evaluate gas tightness of the obtained dense functional layer showed no detectable He leakage endorsing the absence of processing defects within it.

In order to increase the surface area available for surface exchange reactions to take place, the surface modification was performed on ∼15 μm thick LSFTa layers. To elevate surface corrugation the approach based on deposition of a second layer of suspension containing pore former (starch) deposited on presintered membranes was performed. As seen from Fig. 9, the presence of high quantity of pore former in deposited layer resulted in extended porosity after the final sintering step. Particles which were in close contact with presintered layer were capable to fully densify, increasing the dense layer thickness by 4–5 μm (Fig. 9a). Although this will result in final dense LSFTa layer thicknesses above 20 μm this is still considered favorable due to the possible defect recoating effect, thus further assuring gas tightness of the membranes. The large pores generated by pore former in upper part of porous layer remained within the final sintered microstructure causing the formation of a "coral type" surface structure (Fig. 9b) with enhanced surface area. Fig. 9 shows that surface structuring on a scale less than 1 μm is possible by the simple approach of dip coating in a suspension containing a pore former.

Oxygen permeation study[20] performed on these membranes showed oxygen flow rates up to ∼8.7 ml cm^{-2} min^{-1} at 1000 °C, where ∼50% increase in oxygen permeation rate was reached due to surface structuring.

5. Conclusions

$La_{0.2}Sr_{0.8}Fe_{0.8}Ta_{0.2}O_{3-\delta}$ composition layers were deposited on porous substrates of the same composition. Deposition was performed by a dip coating technique using colloidal suspensions electro-steric stabilized with an optimum quantity of a polymeric based commercial surfactant. Optimum quantity of

the surfactant was found to be 2.5 wt.%, determined by evaluating $La_{0.2}Sr_{0.8}Fe_{0.8}Ta_{0.2}O_{3-\delta}$ composition particle surface charge, size evolution and colloidal system rheological response.

Dense and defect free layers within thickness in the range of 15–60 μm were obtained by a single dip coating deposition. By employing small initial particles the grain size was kept in the sub-micron range also after the final thermal treatment step. Deposition of a second layer with pore former resulted in a significantly enhanced surface area of the functional layer.

Acknowledgements

The authors acknowledge the funding provided by the Norwegian Research Council (NFR), FRINAT-project no. 191358: The kinetics of surface exchange reactions in oxide based mixed conductors at reducing conditions and high temperatures.

References

1. Bouwmeester HJM. Dense ceramic membranes for methane conversion. *Catal Today* 2003;**82**(1–4):141–50.
2. Kharton VV, Yaremchenko AA, Kovalevsky AV, Viskup AP, Naumovich EN, Kerko PF. Perovskite-type oxides for high-temperature oxygen separation membranes. *J Membr Sci* 1999;**163**(2):307–17.
3. Hendriksen PV, Larsen PH, Mogensen M, Poulsen FW, Wiik K. Prospects and problems of dense oxygen permeable membranes. *Catal Today* 2000;**56**(1–3):283–95.
4. Sunarso J, Baumann S, Serra JM, Meulenberg WA, Liu S, Lin YS, da Costa JCD. Mixed ionic–electronic conducting (MIEC) ceramic-based membranes for oxygen separation. *J Membr Sci* 2008;**320**(1–2):13–41.
5. Hashim SM, Mohamed AR, Bhatia S. Current status of ceramic-based membranes for oxygen separation from air. *Adv Colloid Interfac* 2010;**160**(1–2):88–100.
6. Sadykov V, Zarubina V, Pavlova S, Krieger T, Alikina G, Lukashevich A, et al. Design of asymmetric multilayer membranes based on mixed ionic–electronic conducting composites supported on Ni-Al foam substrate. *Catal Today* 2010;**156**(3–4):173–80.
7. Buchler O, Serra JM, Meulenberg WA, Sebold D, Buchkremer HP. Preparation and properties of thin $La_{1-x}Sr_xCo_{1-y}Fe_yO_{3\text{-delta}}$ perovskitic membranes supported on tailored ceramic substrates. *Solid State Ionics* 2007;**178**(1–2):91–9.
8. Lein HL, Wiik K, Grande T. Kinetic demixing and decomposition of oxygen permeable membranes. *Solid State Ionics* 2006;**177**(19–25): 1587–90.
9. Matsuka M, Agranovski IE, Braddock RD. Preparation of asymmetric perovskite-type membranes by a settlement method. *Ceram Int* 2010;**36**(2):643–51.
10. Reed JS. *Principles of ceramic processing*. 2nd ed. New York: John Willey & Sons; 1994.
11. Bowen P, Carry C. From powders to sintered pieces: forming, transformations and sintering of nanostructured ceramic oxides. *Powder Technol* 2002;**128**(2–3):248–55.
12. Liu DM. Adsorption, rheology, packing, and sintering of nanosize ceramic powders. *Ceram Int* 1999;**25**(2):107–13.
13. Lange FF. Powder processing science and technology for increased reliability. *J Am Ceram Soc* 1989;**72**(1):3–15.
14. Ikeguchi M, Ishii K, Sekine Y, Kikuchi E, Matsukata M. Improving oxygen permeability in $SrFeCo_{0.5}O_I$ asymmetric membranes by modifying support-layer porous structure. *Mater Lett* 2005;**59**(11): 1356–60.
15. Mokkelbost T, Andersen O, Strom RA, Wiik K, Grande T, Einarsrud MA. High-temperature proton-conducting $LaNbO_4$-based materials: powder synthesis by spray pyrolysis. *J Am Ceram Soc* 2007;**90**(11): 3395–400.
16. Paik U, Hackley VA, Choi SC, Jung YG. The effect of electrostatic repulsive forces on the stability of $BaTiO_3$ particles suspended in non-aqueous media. *Colloids Surf, A* 1998;**135**(1–3):77–88.
17. Bartonickova E, Wiik K, Maca K, Lein HL, Rudberg EA. Synthesis and oxygen transport properties of $La_{0.2}Sr_{0.8}Fe_{1-x}Ti_xO_{3\text{-delta}}$ ($x = 0.2$, 0.4) intended for syn-gas production. *J Eur Ceram Soc* 2010;**30**(2): 605–11.
18. Moreno R. The role of slip additives in tape-casting technology 1. Solvents and dispersants. *Am Ceram Soc Bull* 1992;**71**(10):1521–31.
19. Rosen MJ. *Surfactants and interfacial phenomena*. 3rd ed. New Jersey: John Wiley & Sons, Inc.; 2004.
20. Gurauskis J., Lohne Ø.F., Wiik K., $La_{0.2}Sr_{0.8}Fe_{0.8}Ta_{0.2}O_{3\text{-delta}}$ based thin film membranes with surface modification for oxygen production. Solid State Ionics, Special SSI-18 Volume, in press, corrected proof.